JOURNAL OF ENVIRONMENTAL SCIENCES 73 (2018) 20–30

Available online at www.sciencedirect.com

ScienceDirect

www.elsevier.com/locate/jes

JES JOURNAL OF ENVIRONMENTAL SCIENCES

www.jesc.ac.cn

Study of ciprofloxacin removal by biochar obtained from used tea leaves

Jie Li[1,2], *Guangwei Yu*[1,*], *Lanjia Pan*[1,2], *Chunxing Li*[1], *Futian You*[1], *Shengyu Xie*[1,2], *Yin Wang*[1,*], *Jianli Ma*[3], *Xiaofu Shang*[3]

1. *Key Laboratory of Urban Pollutant Conversion, Institute of Urban Environment, Chinese Academy of Sciences, Xiamen 361021, China. E-mail:* jieli@iue.ac.cn
2. *University of Chinese Academy of Sciences, Beijing 100049, China*
3. *Tianjin Huankelijia Environment Remediation Technology Co., Ltd., Tianjin 300191, China*

ARTICLE INFO

Article history:
Received 21 September 2017
Revised 22 December 2017
Accepted 28 December 2017
Available online 7 January 2018

Keywords:
Biochar
Used tea leaves
Ciprofloxacin adsorption
Isotherm
Kinetics
Mechanism

ABSTRACT

In this study, used tea leaves (UTLs) were pyrolyzed to obtain used tea-leaf biochar (UTC), and then the UTC was used as an adsorbent to remove ciprofloxacin (CIP) from aqueous solutions. Batch experiments were conducted to investigate the CIP adsorption performance and mechanism. The results showed that the CIP-adsorbing ability first increased and then declined as the UTC pyrolysis temperature increased. The UTC obtained at 450°C presented excellent CIP-absorbing ability at pH 6 and 40°C. The maximum monolayer adsorption capacity was 238.10 mg/g based on the Langmuir isotherm model. The pseudo-second-order kinetic equation agreed well with the CIP adsorption process, which was controlled by both external boundary layer diffusion and intra-particle diffusion. The characterization analysis revealed that the –OH groups, C═C bonds of aromatic rings, C–H groups in aromatic rings and phenolic C–O bonds play vital roles in the CIP adsorption process, and that the N–C, N–O, O–C═O and C–OH groups of UTC were consumed in large quantities. π–π interactions, hydrogen bonding and electrostatic attraction are inferred as the main adsorption mechanisms. The present work provides not only a feasible and promising approach for UTLs utilization but also a potential adsorbent material for removing high concentrations of CIP from aqueous solutions.

Introduction

Tea leaves are extensively used to provide flavor in beverages. In China, 20% of the domestic beverage market is occupied by the tea beverage industry. It was reported that the output of tea leaves was 2.27 million tons in 2015, and more than 2 million tons of used tea leaves (UTLs) were left after consumption (Shen et al., 2017). The accumulation of UTLs on the ground is a burden to the ecological environment and causes a vast waste of resources (Zhu et al., 2013). Thus, finding an appropriate disposal method for UTLs is extremely urgent. The traditional approach to UTLs treatment is to burn it for thermal energy. However, incineration contributes to environmental pollution, such as greenhouse gases and other forms of air pollution (Bartolozzi et al., 2017).

In addition, ciprofloxacin (CIP), as a third generation fluoroquinolone antibiotic, has become one of the most commonly detected antimicrobial agents due to its widespread application for decades in China (Wang et al., 2016). It has been frequently detected in the excrement of livestock and in soil and water

* *Corresponding authors. E-mails:* gwyu@iue.ac.cn (Guangwei Yu), yinwang@iue.ac.cn (Yin Wang).

https://doi.org/10.1016/j.jes.2017.12.024
1001-0742/

because of its high stability and bacteria-inhibiting effects (Mao et al., 2016). It has been reported that the CIP concentration in wastewater is as high as 31 mg/L, with higher concentrations in the effluents from drug production plants (Zhang et al., 2017). CIP has been proven to be an emerging genotoxic contaminant that can damage ecosystems and human health via its acute and chronic toxicity (Espinosa et al., 2015; Li et al., 2014). Therefore, the removal of CIP from aqueous environments has become an urgent issue. Many approaches have been developed to treat CIP in contaminated water, such as biological, photolytic/photocatalytic, oxidation and adsorption treatments (Diao et al., 2017; Liao et al., 2016; Tu et al., 2014). Among these methods, adsorption technology is considered to be a promising approach based on its simple design, easy operation, relatively simple maintenance and environmental friendliness (Alahabadi et al., 2007).

In recent years, many works have been undertaken to develop alternative and more economical adsorbents. As raw material for adsorbents, biomass-like waste byproducts from large-scale industrial operations and agricultural adsorbents have attracted the interest of investigators (Alahabadi and Moussavi, 2017; Fernandez et al., 2015). Regarding UTLs, some new treatments have been provided to preferably utilize UTLs with higher added value, including its direct use as an adsorbing material and its use as a raw material to prepare active carbon and biochar (Li et al., 2015b; Peng et al., 2013). Among the above approaches, producing biochar by pyrolysis as an adsorbent to remove organic contaminants is a promising choice. Recently, some works have studied the adsorption of organic pollutants, such as carbofuran and sulfamethazine, by biochar derived from UTLs (Vithanage et al., 2016; Rajapaksha et al., 2014). However, little work has been done to investigate the effect of biochar obtained from used tea leaves on the adsorption of ciprofloxacin.

In this study, UTLs were pyrolyzed to produce used tea-leaf biochar (UTC), and then the UTC was used to adsorb CIP. The effects of various operating parameters, including the UTC pyrolysis temperature, contact time, CIP concentration, solution temperature and pH, were investigated in detail. Moreover, the adsorption kinetics and isotherms were studied, and the adsorption mechanism was deduced based on the analysis of the characteristics of UTC before and after CIP adsorption.

1. Materials and methods

1.1. Raw materials and preparation of UTC

Ciprofloxacin (CIP), analytical standard grade, was purchased from the Aladdin Industrial Corporation in Shanghai, China. All other chemicals were obtained from Sinopharm Chemical Reagent Co., Ltd. and were of analytical grade. CIP solutions were prepared at various initial concentrations for the batch adsorption experiments, and Milli-Q water was used in all experimental procedures.

The used tea leaves (UTLs) were collected from Fujian Xian Yang Yang Food & Technology Co., Ltd., Ningde City of Fujian province, China. The UTLs were ground and sieved through a 100-mesh sieve after drying and then stored in a clean airtight container. Detailed information about UTLs was obtained via proximate and ultimate analysis. The dry-based contents of ash, volatiles and fixed carbon in UTLs were 4.88, 72.98 and 22.14 wt.%, respectively, and the base dry-ash-free contents of H, C, N, O and S were as follows: 4.46, 48.05, 3.12, 43.74 and 0.63 wt.%, respectively.

The UTLs were pyrolyzed at five different pyrolysis temperatures (350, 400, 450, 500 and 550°C) for 30 min with a ramp rate of 10°C/min in a vertical tubular furnace under nitrogen atmosphere (Fig. 1). The solid pyrolysis product, UTC, was ground after cooling down and then screened through a 200-mesh sieve; subsequently, the samples were stored in clean airtight containers until they were used for subsequent experiments.

1.2. Adsorption tests and detection of CIP

1.2.1. Adsorption tests of CIP

Batch adsorption experiments were conducted by adding 0.2 g of UTC to 150 mL of the CIP solution in sealed conical flasks. The sealed conical flasks were placed in a temperature-controlled light-protected shaker at a speed of 200 r/min for 24 hr. The samples collected during the batch adsorption experiments were filtered through a 0.45 μm membrane before detection. All the measurements were repeated three times, and the error was calculated to support the data accuracy.

The effects of the experimental conditions on CIP adsorption were investigated as follows.

(1) Six different initial concentrations (150, 200, 250, 300, 400 and 500 mg/L) were selected to study the effect of the CIP concentration. The pH and temperature of the CIP solutions were 6 and 30°C, respectively.
(2) To investigate the effect of the contact time, samples were withdrawn at different time intervals during the 24 hr period. The adsorption experiments were conducted at pH 6 and 30°C for CIP solutions at three different concentrations (150, 200 and 250 mg/L).
(3) The effects of the solution temperature on absorption were studied at 30, 35, 40, 50 and 60°C at pH 6 and with an initial CIP concentration of 200 mg/L.
(4) The effects of pH on the CIP adsorption were determined using samples with an initial CIP concentration of 200 mg/L at 30°C. The pH of the sample solutions was adjusted to different values (4, 5, 6, 7, 8 and 10) using 0.1 mol/L NaOH or 0.1 mol/L HCl.

1.2.2. Models of the adsorption kinetics and isotherms

The pseudo-first-order model, pseudo-second-order model and intra-particle diffusion model (Nasuha et al., 2010) were selected to determine the adsorption kinetics of CIP by UTC based on the experimental adsorption data from various contact times.

To identify the adsorption behavior of the CIP molecules with UTC, the equilibrium isotherm data at six different initial CIP concentrations were modeled using the Langmuir, Freundlich and Dubinin–Radushkevich (D–R) isotherm equations individually (Fan et al., 2016).

1.2.3. Detection of CIP

The CIP concentration in the filtrate was detected with high-performance liquid chromatography (HPLC, L-2000, Hitachi, Japan) at a column temperature of 30°C and wavelength of

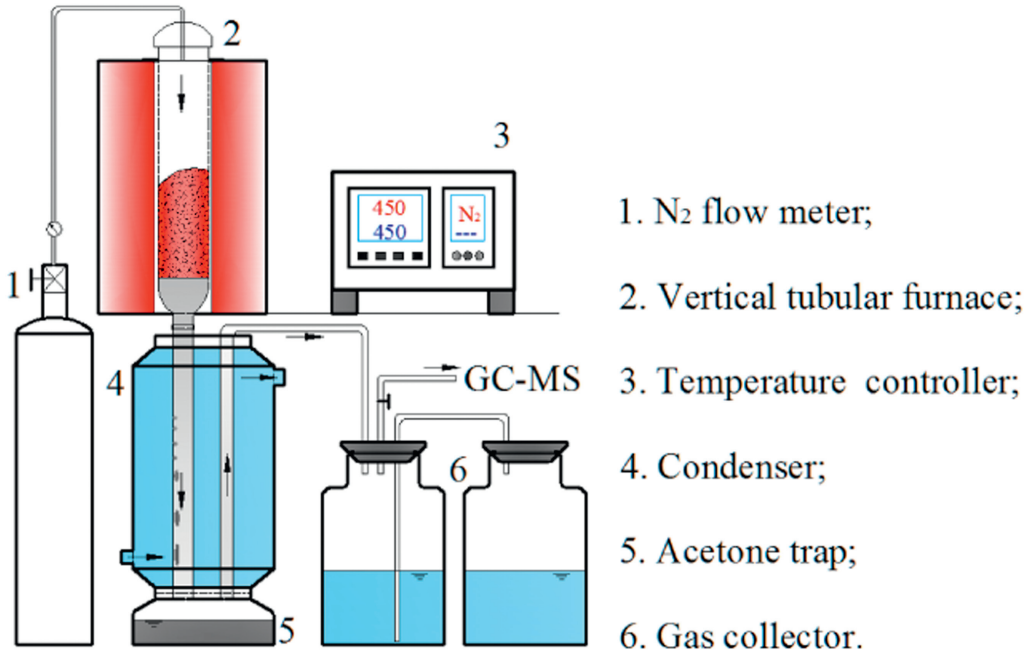

Fig. 1 – Schematic diagram of the pyrolysis apparatus. GC–MS: gas chromatography-mass spectrometer.

278 nm. An Extend-C18 column (250 mm × 9 4.6 mm, 5-Micron 80A, Agilent, USA) was used to achieve the chromatographic separation. The mobile phases were trichloroacetic acid (0.02 mol/L), acetonitrile and methanol (74/22/4, V/V/V). The amount of adsorption (q_t) at the contact time (t), the amount of absorption at equilibrium (q_e), and the removal percentage (R) of CIP were calculated *via* Eqs. (1)–(3), respectively.

$$q_t = (C_0 - C_t) \times V/W \quad (1)$$

$$q_e = (C_0 - C_e) \times V/W \quad (2)$$

$$R = (C_0 - C_e) \times 100/C_0 \quad (3)$$

where t (hr) is the contact time, q_t and q_e (mg/g) are the amounts of CIP adsorption at t and at equilibrium, respectively, R (%) is the removal efficiency of CIP, C_0 and C_e (mg/L) are the initial and equilibrated concentrations of CIP, respectively, V (L) is the volume of the solution and W (g) is the mass of the UTC.

1.3. Characterization

To determine the zeta potential of UTC, approximately 0.01 g of each sample was ball-milled in an agate jar that contained 200 mL of a 0.1 mmol/L NaCl solution. The suspensions were dispersed ultrasonically after adjusting the pH in the range of 2–9 using 0.1 mol/L NaOH or 0.1 mol/L HCl. The samples were measured using a Zetasizer Nano ZS (Zeta PALS, Malvern, UK) after standing for 24 hr.

The pore-size distributions and specific surface areas of the samples were analyzed according to the nitrogen adsorption/desorption isotherms measured in a volumetric system (ASAP 2020 M + C, Micromeritics, USA). Prior to N_2 adsorption, all the samples were degassed at 200°C for 12 hr. The Brunauer–Emmett–Teller (BET) method was applied for the specific surface area calculation because it is more suitable for samples with typical type IV adsorption/desorption isotherms.

For testing the surface morphology of the samples, scanning electron microscopy (SEM, S-4800, Hitachi, Japan) was applied with voltage and current settings of 5 kV and 10 mA, respectively.

Fourier transform infrared spectroscopy (FTIR, iS10, Thermo, USA) was used to determine the surface functional groups with the spectra recording from 4000 to 400 cm^{-1}.

Surface species of the samples were analyzed by X-ray photoelectron spectroscopy (XPS, EscaLab250Xi, Thermo Fisher Scientific, UK) with monochromatic Al-*K* radiation (15 kV, 150 W). The instrument base pressure was 10^{-9} Torr, and high-resolution spectra were collected over an analysis area of 500 μm × 500 μm.

2. Results and discussion

2.1. Effect of the UTC pyrolysis temperature on the CIP adsorption

The UTC obtained from five different pyrolysis temperatures was used for CIP adsorption (Fig. 2). The amount of CIP adsorbed at equilibrium (q_e) first increased and then decreased with the increase in the pyrolysis temperature from 350 to 550°C. The removal percentage of the CIP (R) presented a similar trend to that of q_e. The result implies that pyrolysis temperature has a significant effect on CIP adsorption. Pyrolysis temperature is an important factor influencing the pore structure and functional groups of biochar, which are vital characteristics for adsorption (Angin, 2013). A lower pyrolysis temperature may result in insufficient functional groups and pore structure in UTC, whereas pore widening and the coalescence of neighboring pores seem to predominate at

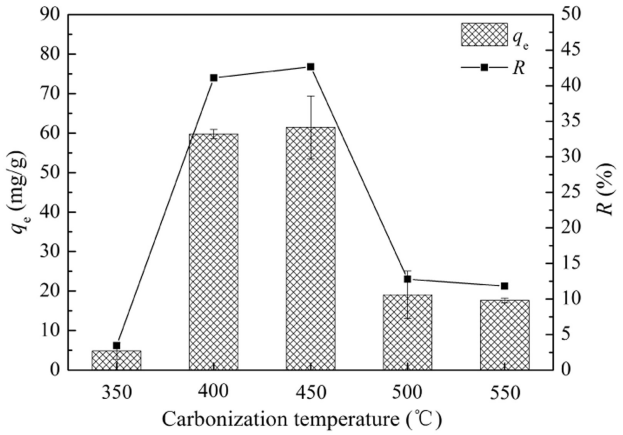

Fig. 2 – Amount of ciprofloxacin (CIP) adsorption at equilibrium (q_e) and removal efficiency of CIP (R) by used tea-leaf biochar (UTC) pyrolyzed at different temperatures.

higher pyrolysis temperatures. Additionally, the functional groups probably disappear via graphitization at high temperatures, which may weaken the adsorption ability as well (Angin, 2013). In the present work, the UTC pyrolyzed at 450°C possessed relatively outstanding adsorption ability, and the value of q_e was 61.44 mg/g. Therefore, the UTC pyrolyzed at 450°C was selected for further study to investigate the CIP adsorption properties and mechanism.

2.2. Effects of the experimental conditions on CIP adsorption

2.2.1. Effects of the contact time on CIP adsorption

Fig. 3a presents the CIP adsorption amount (q_t) with the contact time (t). The value of q_t increased rapidly for the first 6 hr and thereafter rose at a slower rate. The equilibrium state was reached after approximately 9 hr. The fast speed of adsorption in the initial time may be caused by the abundant free active sites on the UTC and high concentration gradient from the liquid to the surface of the UTC (Chang et al., 2014; Cheung et al., 2007).

2.2.2. Effects of the initial CIP concentration on the CIP adsorption

As shown in Fig. 3b, the initial CIP concentration plays an important role in the amount of the CIP adsorbed by UTC. As seen in the figure, the amount of CIP adsorbed on the UTC at equilibrium increased from 32.9 to 146.9 mg/g with the increase in the CIP concentration from 150 to 500 mg/L; the maximum removal efficiency (R) of CIP was achieved when the initial concentration of CIP was 200 mg/L. The results indicate that q_e and R initially increase and then decrease with the increase in the initial CIP concentration. Yang et al. (2010) reported a similar result regarding the effect of the zinc ion concentration on the biosorption of zinc by dried activated sludge. A possible reason for q_e elevation is that the higher concentration provides a stronger driving force, *i.e.*, the adsorption concentration gradient, to overcome the resistance of the CIP transfer between the aqueous and solid phases (Srivastava et al., 2006). The subsequent decrease in the removal efficiency of CIP at a higher initial concentration may be caused by insufficient binding sites on UTC for the adsorption (Yang et al., 2010).

2.2.3. Effect of the solution temperature on CIP adsorption

The effect of the solution temperature on CIP adsorption by UTC is shown in Fig. 3c. The value of q_e increased from 61.4 to 67.7 mg/g as the temperature increased from 30 to 40°C.

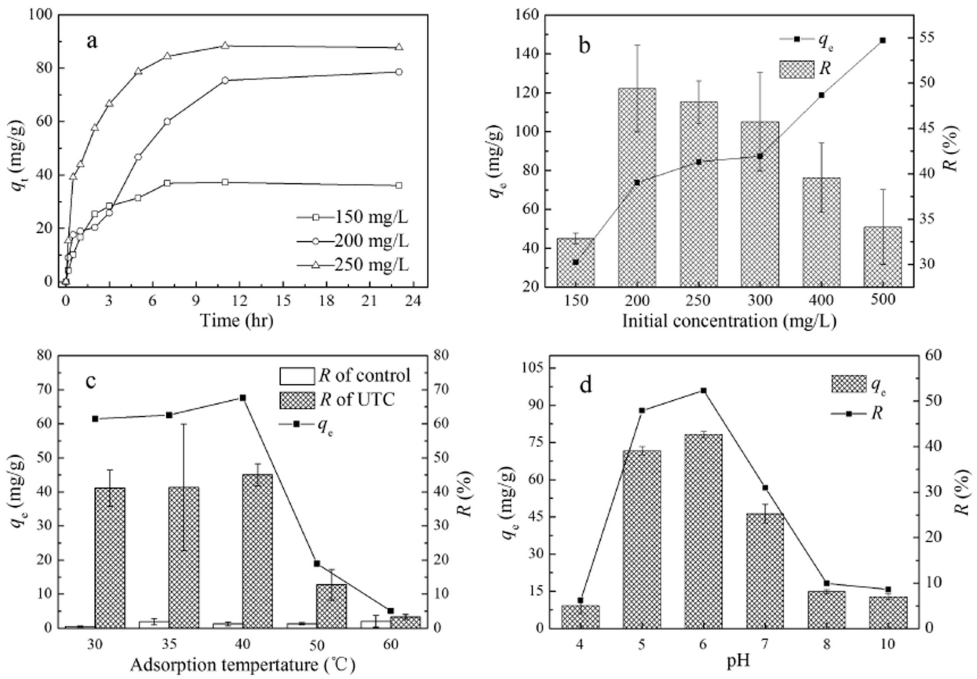

Fig. 3 – (a) Effects of the contact time, (b) initial CIP concentration, (c) adsorption temperature and (d) pH on CIP adsorption by UTC. q_t: the adsorption amount at time t.

However, when the temperature increased from 40 to 60°C, the CIP adsorption of UTC decreased dramatically. The best adsorption temperature was 40°C. The reason for this result may be easier penetration of the CIP molecules into the external boundary layer and internal pores of the UTC due to the increase in the number of adsorptive sites and the diffusion mobility at the appropriate adsorption temperature (Ghasemi and Asadpour, 2007). Alternatively, the adsorbate molecules tend to escape from the solid phase with an increase in the temperature of the solution (Gupta et al., 2011). Therefore, when the temperature of the solution is higher than 40°C, the CIP molecules may be too active to be trapped by the pores and functional groups, leading to a decrease in q_e.

2.2.4. Effect of the solution pH on CIP adsorption

As illustrated in Fig. 3d, the solution pH has a significant influence on the q_e of the UTC. The q_e increased sharply to 78.24 mg/g at pH 6 and then decreased rapidly at pH 8. A similar variation trend was obtained by El-Shafey et al. (2012). UTC has an amphoteric character that depends on the solution pH. Fig. 4b shows that the pH at the point of zero charge (pH_{PZC}) of UTC is 3.05. When $pH > pH_{PZC}$, the UTC surface is negatively charged, whereas it is positively charged at $pH \leq pH_{PZC}$. In addition, CIP exists as CIP^+ at pH < 5.9 ± 0.15, $CIP^{\pm}$ and CIP^0 at pH values from 6.1 to 8.7, and CIP^- at pH > 8.89 ± 0.11 (Peng et al., 2015), as described in Fig. 4a. When the solution pH is between 5 and 6, the UTC surface is strongly electronegative, and CIP predominantly exists as a cationic species, which results in the observed strong CIP adsorption capacity on UTC (Fig. 3b). The testing results showed that the strongest CIP adsorbing ability was obtained at a pH of 6.

2.3. Adsorption kinetics studies

To study the adsorption kinetics of CIP by UTC, the pseudo-first-order model (Eq. (4)), pseudo-second-order model (Eq. (5)) and intra-particle diffusion model (Eq. (6)) were used, and their equations are given as follows (Nasuha et al., 2010):

$$\log(q_e - q_t) = \log q_e - k_1\, t/2.303 \tag{4}$$

$$t/q_t = 1/(k_2\, q_e^{\,2}) + t/q_e \tag{5}$$

$$q_t = k_{id}\, t^{1/2} + C \tag{6}$$

where t (hr) is the contact time of adsorption, q_e and q_t (mg/g) are the amounts of CIP adsorbed at equilibrium and at t, respectively, k_1 (hr^{-1}) is the rate constant of the pseudo-first-order model, k_2 (g/(mg·hr)) is the rate constant of the second-order model, k_{id} (mg/(g·$hr^{1/2}$)) is the diffusion rate constant of the intra-particle model, and C indicates the thickness of the boundary layer.

To compare the applicability of the models for fitting the data quantitatively, a normalized standard deviation, Δq (%), was calculated according to the following equation (Nasuha et al., 2010):

$$\Delta q = 100 \times \left(\sum \left(\left(q_{t,\,exp} - q_{t,cal} \right) / q_{t,\,exp} \right)^2 / (n-1) \right)^{1/2} \tag{7}$$

where $q_{t,exp}$ and $q_{t,cal}$ (mg/g) refer to the experimental and calculated values, respectively, at contact time t, and n is the number of data.

The results fitted with different kinetic models of CIP adsorption on UTC are shown in Fig. 5a–b and Table 1. The value of R^2 for the pseudo-second-order model was greater than 0.94, which was much closer to 1 than that of the pseudo-first-order model. The $q_{e,cal}$ of the pseudo-second-order model fit well with $q_{t,exp}$, and the Δq value was smaller. The above results suggest that the pseudo-second-order kinetic model appears to be a better fit for CIP adsorption on UTC, which is similar to the results of the study by He et al. (2017). This indicates that chemical adsorption is involved during the adsorption process, and the adsorption capacity is proportional to the number of active sites (Li et al., 2015a).

The intra-particle diffusion model was used to investigate the diffusion mechanism of the adsorption process (Fig. 5c). It was observed that the adsorption process tended to be divided into two linear portions over the total time. The first sharper portion is attributed to the diffusion of CIP to the external surface of UTC. The second portion describes a gradual adsorption stage in the micropores and mesopores of UTC, indicating that a greater resistance occurred during this stage and that the diffusion of CIP into the UTC pores is a slow process (He et al., 2017).

The adsorption diffusion mechanism has been well illustrated as consisting of three steps (Cheung et al., 2007): (1) outer diffusion/boundary layer diffusion: mass transfer across the external boundary layer film; (2) inner diffusion/intra-particle diffusion: diffusion of adsorbate molecules into the pores and active sites of the adsorbent by pore diffusion or solid-surface diffusion; (3) adsorption at sites on the external or internal surface of the adsorbents. One or a combination of the three can be the rate-limiting step, but the third step cannot be considered the rate-limiting step

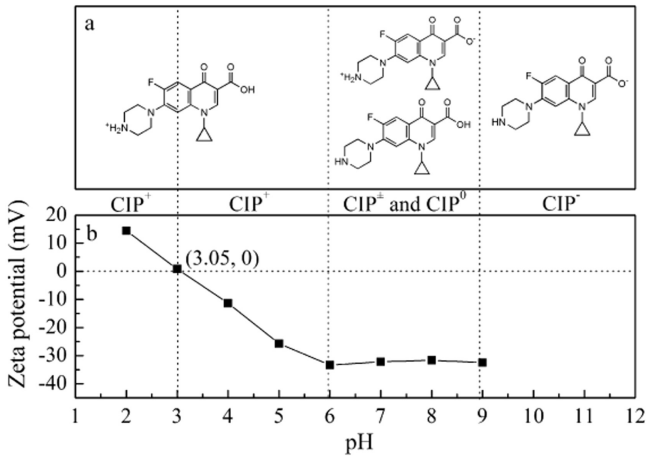

Fig. 4 – (a) Speciation of CIP and (b) zeta potential of UTC at different pH values.

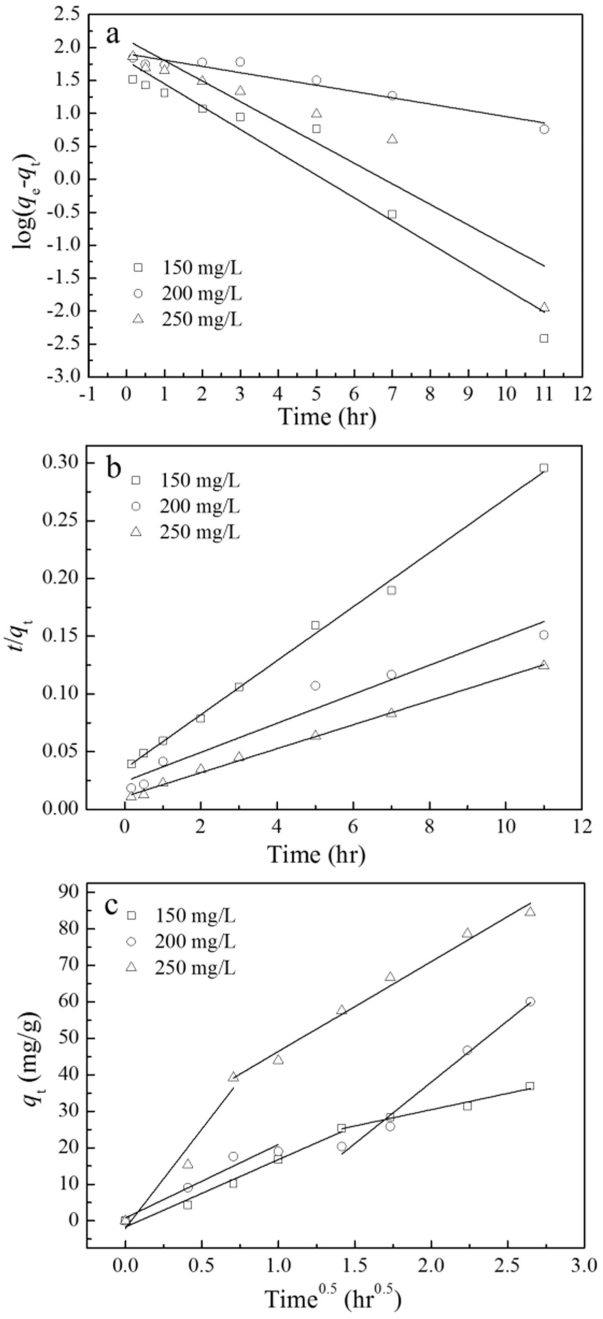

Fig. 5 – Kinetic model fittings of the adsorption of CIP by UTC: (a) pseudo-first, (b) pseudo-second, and (c) intra-particle diffusion models.

because of its high speed. Hence, the absorption rate is controlled by outer diffusion, inner diffusion, or both (Sun et al., 2016). The first linear portion corresponded to the boundary layer diffusion, and the second linear portion accounted for the intra-particle diffusion. In the present study, the first linear portion of the plots did not pass through the origin (Fig. 5c), suggesting that intra-particle diffusion was not the unique rate-controlling step, and that the boundary layer diffusion also partially controlled the adsorption.

Table 1 – Kinetic parameters for the removal of ciprofloxacin (CIP) by the used tea-leaf biochar (UTC).

Kinetic models	Parameters	C_0 (mg/L)		
		150	200	250
Pseudo-first-order parameters	$q_{e,exp}$ (mg/g)	37.20	78.56	88.39
	k_1 (hr^{-1})	0.80	0.22	0.72
	$q_{e,cal}$ (mg/g)	62.62	80.28	130.45
	R^2	0.93	0.92	0.87
	Δq (mg/g)	89.29	36.56	52.36
Pseudo-second-order parameters	$q_{e,cal}$ (mg/g)	42.79	79.49	96.34
	k_2 (g/(mg·hr))	0.02	0.01	0.01
	R^2	1.00	0.94	1.00
	Δq (mg/g)	4.76	47.90	10.00
Intra-particle diffusion parameters	k_{id1} (mg/(g·$hr^{1/2}$))	18.44	20.10	54.34
	C_1	−1.68	0.80	−2.03
	R_1^2	0.98	0.93	0.91
	k_{id2} (mg/(g·$hr^{1/2}$))	8.92	33.64	24.67
	C_2	12.61	−29.27	21.67
	R_2^2	0.96	0.98	0.98

$q_{e,exp}$: experimental values; k_1: rate constant of the pseudo-first-order model; $q_{e,cal}$: calculated values; Δq: normalized standard deviation; k_2: rate constant of the second-order model; k_{id1}: diffusion rate constant of the intra-particle model in the first portion; C_1: thickness of the boundary layer in the first portion; k_{id2}: diffusion rate constant of the intra-particle model in the second portion; C_2: thickness of the boundary layer in the second portion; C_0: initial concentrations of CIP.

2.4. Adsorption isotherm studies

The equations of the Langmuir, Freundlich and Dubinin-Radushkevich (D-R) isotherm models are given as follows (Fan et al., 2016):

$$\text{Langmuir isotherm equation}: C_e/q_e = 1/(q_{max}K_L) + C_e/q_{max} \quad (8)$$

$$R_L = 1/(1 + K_L C_0) \quad (9)$$

$$\text{Freundlich isotherm equation}: \ln q_e = \ln K_F + \ln C_e/n_e \quad (10)$$

$$\text{D–R adsorption isotherm equation}: \ln q_e = \ln q_m - \beta\varepsilon^2 \quad (11)$$

$$\varepsilon = RT \ln(1 + 1/C_e) \quad (12)$$

$$E_a = 1/(2\beta)^{1/2} \quad (13)$$

where C_e and C_0 (mg/L) are the equilibrium and initial concentrations of CIP, respectively; q_e (mg/g) is the adsorption capacity at equilibrium; K_L (L/g) is the Langmuir constant; q_{max} (mg/g) is the maximum adsorption capacity; R_L is the dimensionless equilibrium parameter; K_F is the Freundlich constant; $1/n_e$ is the heterogeneity of the sorption sites and an indicator of isotherm nonlinearity; q_m (mg/g) is the theoretical isotherm saturation capacity; β and ε are D–R constants; and E_a (kJ/mol) is the free energy of adsorption.

The regression coefficients indicate that both the Langmuir (R^2 = 0.99) and Freundlich (R^2 = 0.99) models fit the adsorption process well. It can be concluded that the adsorption process is monolayer adsorption on a heterogeneous surface (Fan et al., 2016; Nasuha et al., 2010). Based on the Langmuir isotherm,

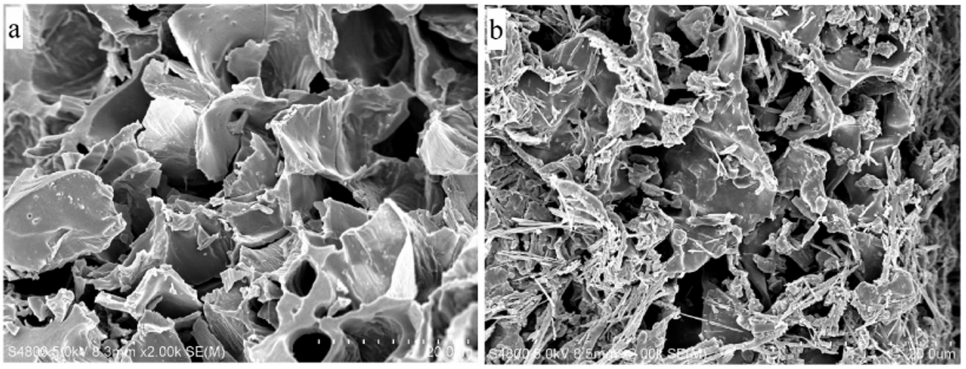

Fig. 6 – Scanning electron microscopy (SEM) micrograph of UTC (a) before and (b) after CIP adsorption.

$0 < R_L < 1$ indicates favorable adsorption (Peng et al., 2016). In this investigation, R_L was 0.32, which indicated that the CIP adsorption process by UTC was favorable. The maximum adsorption capacity (q_{max}) obtained from the Langmuir isotherm was 238.10 mg/g. The type of adsorption can be estimated from the E_a of the D–R model, and when E_a is in the range of 16–40 kJ/mol, the process is chemical adsorption (Sun et al., 2016; Peng et al., 2016). Hence, the CIP adsorption by UTC was mainly through chemisorption because the value of E_a was 25.48 kJ/mol.

2.5. *Characteristics of UTC before and after adsorption*

Fig. 6 presents the SEM micrographs of UTC before and after adsorption. As shown in Fig. 6a, UTC possessed a rugged surface with non-uniform pores. The average pore diameter (D_a), the cumulative volume of the pores (V_{total}) and the BET surface area (S_{BET}) of UTC were 4.44 nm, 0.012 cm^3/g and 8.06 m^2/g, respectively. Uzun et al. (2010) have synthesized fuel products (bio-oil and bio-char) from tea waste, and the bio-char produced at 973 K had a relatively low surface area of 7.5 m^2/g, which was close to our result. However, for UTC after the CIP adsorption (UTC_{ad}), a mass of rod and block-shaped particles appeared in the pores and on the surface (Fig. 6b). The above results indicate that CIP adsorption by UTC is related to the pore structure and is also affected by the components of the functional groups on the UTC surface (Han et al., 2016).

The FTIR spectra were analyzed to identify the characteristic functional groups of the adsorbents. The 4000–400 cm^{-1} infrared spectral regions of the UTC and UTC_{ad} are shown in Fig. 7. Several obvious peaks can be observed in the infrared spectra of UTC. As shown in Table 2, the functional groups, including the stretching vibrations of –OH (3400 cm^{-1}), the C═C bond in an aromatic ring or C═C bond (1570 cm^{-1}), C–H alkanes (1435 cm^{-1}) and C–O in phenol (1167 cm^{-1}), are clearly identified. Two other weak peaks at 2917 and 2850 cm^{-1} are related to the symmetric and asymmetric stretching vibrations of methylene (Huang et al., 2015; Malkoc and Nuhoglu, 2006; Sun et al., 2016).

Compared to the infrared spectra of UTC, some new peaks appeared, and some peaks shifted in the infrared spectra of UTC_{ad}. The new peaks at 3038, 1490, 1384, 1335, 1309, 1271 and

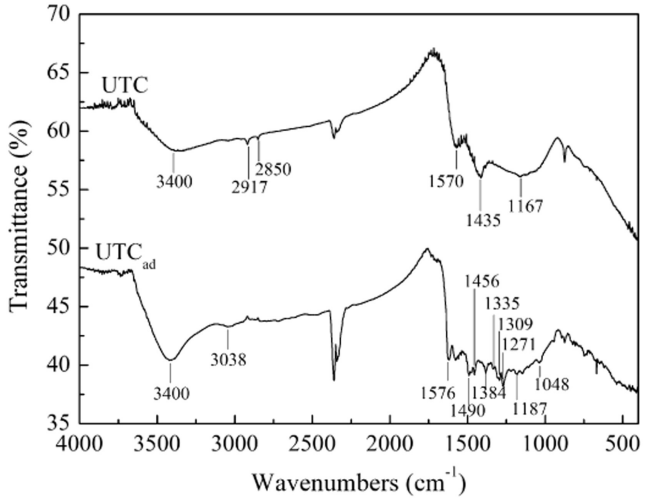

Fig. 7 – Fourier transform infrared spectroscopy (FTIR) spectra of used tea-leaf biochar before (UTC) and after (UTC_{ad}) CIP adsorption.

Table 2 – Fourier transform infrared spectroscopy (FTIR) spectral characteristics of used tea-leaf biochar before (UTC) and after (UTC_{ad}) CIP adsorption.

UTC (cm^{-1})	UTC_{ad} (cm^{-1})	Functional groups
3400	3413	Stretching vibrations of –OH groups
	3038	N–H stretching vibration
2917		Aliphatic CH_2 asymmetric stretch
2850		Aliphatic CH_2 symmetric stretch
1570	1576	C═C band of the aromatic ring or highly conjugated C═C bond
	1490	Secondary amine group
1435	1456	Symmetric bending of CH_3
	1384	Bending vibration of methyl
	1335	Aromatic nitro compound
	1309	C–H stretching vibration
	1271	Phenolic C–OH stretch
1167	1187	C–O in phenol
	1048	C═O stretching

1048 cm^{-1} are assigned to the N–H stretching vibrations, secondary amine groups, bending vibrations of methyl, aromatic nitro compounds, C–H stretching vibrations of phenolic C–OH stretch and C═O stretching, respectively (Chang et al., 2014; Eroglu et al., 2009; Fan et al., 2016; Moniruzzaman and Ono, 2013; Nasuha et al., 2010; Trivedi and Vasudevan, 2007). The new functional groups that appeared on the surface of UTC_{ad} probably originated from the CIP molecules. Moreover, compared with UTC, the band frequencies of UTC_{ad} displayed a significant change in the sorption bands at 3400, 1570, 1435, and 1167 cm^{-1}. This indicates that the –OH groups, the C═C bonds of the aromatic rings, the C–H groups in aromatic rings and the C–O in the phenol bonds play vital roles in the CIP adsorption by UTC.

Furthermore, the characteristics of F 1s, C 1s, O 1s and N 1s energies for UTC and UTC_{ad} were determined by XPS (Table 3), providing information on the surface interactions and chemical state of the elements. The peak of F ls at 686.68 eV has been suggested to be an indicator to estimate whether CIP is absorbed by UTC because F only exists in the CIP molecule. The F ls XPS spectra of CIP, UTC and UTC_{ad} are shown in Fig. 8. The figure shows that the F ls peak is only found on UTC_{ad} and CIP, demonstrating that the CIP was absorbed by UTC.

Fig. 9a shows the C 1s XPS spectra of UTC and UTC_{ad}. For UTC, the peak at 284.50 ± 0.25 eV is associated with C–C, C–H aromatic, or aliphatic hydrocarbons (Shen et al., 2017). For peak 3 in the figure, the binding energy was 285.20 eV, corresponding to C═O or C–O–C groups. The C–N and C═N structures were also identified at a very similar binding energy. The peak at 286.35 eV proves the existence of C–OH or C≡N (Dementjev et al., 2000; Jiang et al., 2013; Shen et al., 2017). Compared with UTC, a new peak, corresponding to N–C═O and C═O in carbonyl, quinine or ketone groups, appears at 287.20 eV for the C 1s of UTC_{ad} (Jiang et al., 2013; Zhang et al., 2014). The generated N–C═O is probably due to the combination of N–H groups in CIP and the C═O groups from UTC. Moreover, the content of peak 3 increased by 14.23% after the CIP adsorption, probably because of the addition of C═O, C–N and C–O–C. The additional content of C–O–C may be generated by the interaction of C–H from UTC and COOH from CIP.

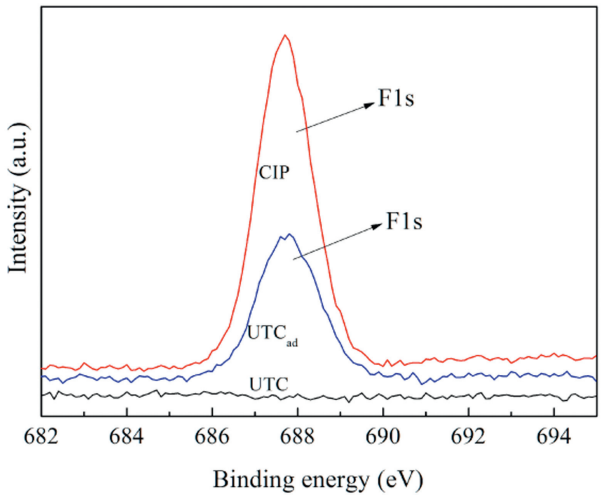

Fig. 8 – F 1s XPS spectra of CIP, used tea-leaf biochar before (UTC) and after (UTC_{ad}) CIP adsorption. XPS: X-ray photoelectron spectroscopy.

The N 1s XPS spectra of UTC and UTC_{ad} are presented in Fig. 9b. Three peaks of N 1s in UTC at 398.70, 400.13 and 400.96 eV are identified as N≡C (or N–C), C–N–C and N–O bonds, respectively (Dementjev et al., 2000). Regarding UTC_{ad}, the N 1s XPS spectra can be separated into four peaks. A new peak is obtained at 401.16 eV, which is assigned to quaternary N (Kicinski et al., 2014). This group probably originates from CIP adsorbed by UTC. Furthermore, it was found that the N≡C (or N–C) and N–O were consumed during the CIP adsorption process because peaks 1 and 3 decreased by 26.03% and 14.24%, respectively.

Fig. 9c shows the O 1s XPS spectra for UTC and UTC_{ad}. The peak at 531.32 eV (or 531.57 eV) represents C═O (or O–C═O). The peak of C–O–C epoxy (or C–OH) emerged at 532.40 eV (or 532.37 eV), and C–O can account for the peak that occurred at 533.58 eV (or 533.42 eV) (Plomp et al., 2009; Shen et al., 2017). After CIP adsorption, a new peak appeared at 530.85 eV which represents C═O (Pang et al., 2010). Moreover, the height of peaks 2 and 3 decreased significantly in UTC_{ad}, indicating the

Table 3 – Relative content of the functional groups of used tea-leaf biochar before (UTC) and after (UTC_{ad}) CIP adsorption.

Element	Peak	UTC		UTC_{ad}		Functional groups
		Position (eV)	Content (%)	Position (eV)	Content (%)	
F 1s	1	ND	0	686.68	100	–F
C 1s	1	284.34	43.83	284.23	26.61	C–C, C–H
	2	284.75	21.91	284.55	14.36	C–C, C–H
	3	285.2	26.15	285.16	40.38	C═O, C–O–C, C–N, C═N
	4	286.35	8.12	286.35	16.05	C–OH, C≡N
	5	ND	0	287.20	2.60	C═O, N–C═O
N 1s	1	398.7	33.75	398.59	7.72	N≡C, C–N
	2	400.13	42.97	399.85	62.36	C–N═C
	3	400.96	23.27	400.90	8.98	N–O
	4	ND	0	401.16	20.94	NC_3
O 1s	1	ND	0	530.85	25.28	C═O
	2	531.32	34.27	531.57	27.80	C═O, O–C═O
	3	532.4	37.47	532.37	22.79	C–O–C, C–OH
	4	533.58	28.26	533.42	24.13	C–O

ND: not detected.

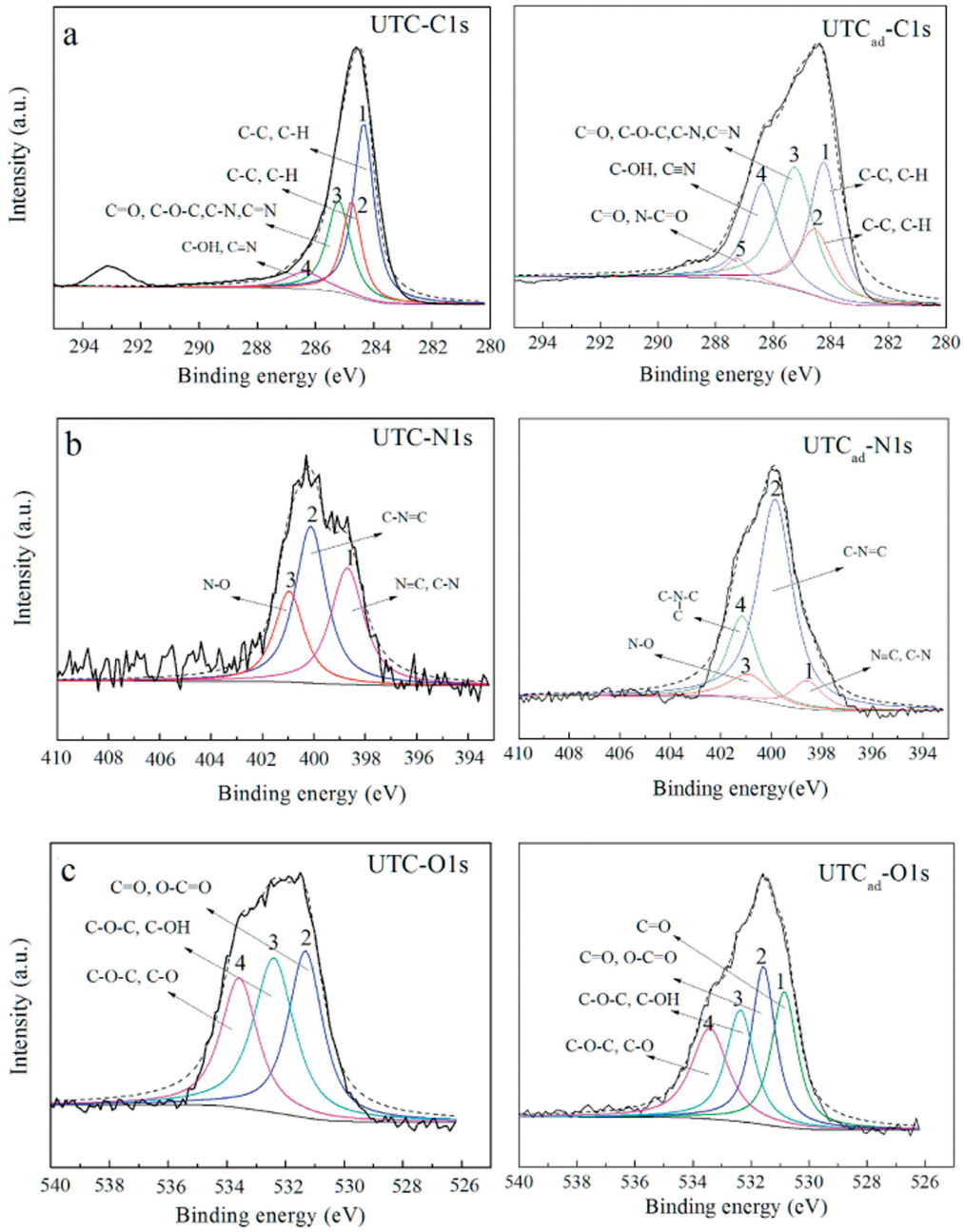

Fig. 9 – (a) C 1s, (b) N 1s and (c) O 1s XPS spectra of used tea-leaf biochar before (UTC) and after (UTC$_{ad}$) CIP adsorption.

consumption of O–C═O and C–OH in UTC during the CIP adsorption.

2.6. Adsorption mechanism analysis

According to the FTIR and XPS analysis, it can be concluded that the –OH groups, C═C bonds of the aromatic rings, C–H groups in aromatic rings and phenolic C–O bonds participated in CIP adsorption by UTC. Furthermore, the N–C, N–O, O–C═O and C–OH of UTC were consumed in large quantities during the adsorption process. In fact, the adsorption mechanism of CIP can be deduced based on the above results.

The chemical bonds (C═C, C–H and C–O) of the aromatic rings and phenol groups in UTC were detected by FTIR. This suggests that UTC mainly consists of aromatics, and π–π interactions may occur during the adsorption process. Han et al. reported that pyrochars formed at 450 and 600°C mainly consist of aromatics and aromatic π systems, which play a primary role in the adsorption of organic pollutants (Han et al., 2016). Aromatic π systems act as π acceptors because of their enrichment in electron-withdrawing functional groups, and the hydroxyl groups on the adsorbents make them electron donors (Han et al., 2016; Keiluweit and Kleber, 2009). A CIP molecule possesses two aromatic heterocyclic groups and one benzene ring a fluorine

group. The fluorine group connected to the benzene ring has a strong electron-withdrawing ability, which causes the aromatic ring to be electron-deficient and act as a π-acceptor (Yang et al., 2012). Moreover, the $-NH_2$ in the aromatic heterocyclic groups may act as an electron-donating group (Han et al., 2016). Therefore, the π–π interactions between the donor–acceptor, donor–donor, or acceptor–acceptor combinations could partially account for the physical sorption capacity of UTC for CIP. In addition, hydrogen-bonding interactions can also take place during the physical adsorption process (Yang et al., 2012). The CIP molecule, which is similar to enrofloxacin, contains several moieties capable of participating in H-bonds as acceptors and donors, which may form H–bonds with the functional groups on the surface of UTC. The benzene ring and other groups (such as C–OH, COOH and N–OH) on the surface of UTC may interact with the functional groups of the CIP molecules through H-bonds. The effectiveness of multiple H-bonds could further improve the adsorption ability.

Another adsorption mechanism is electrostatic interactions between the functional groups on the UTC_{ad} surface and the CIP molecules. The aforementioned results suggest that those chemical bonds, including C–O, O–C═O, N–O and C–N, play vital roles in the adsorption process because of their depletion. Furthermore, the solution pH can affect the electrostatic interactions during CIP adsorption by UTC. When $pH > pH_{pzc}$ (3.05), the –CO–, –COO–, N–O– and C–N– groups appear via hydrogen ion release (Fan et al., 2016). When $3.05 < pH < 5.9 \pm 0.15$, these functional groups in UTC possess potentials opposite to that of CIP^+, contributing to the electrostatic attractions between them. The optimum adsorption capacity of CIP was obtained at a pH between 5 and 6, as described in Fig. 3d. When the pH < 5, the amounts of –CO–, –COO–, N–O– and –CN– decrease markedly, leading to a reduction in the CIP adsorption. When the pH > 6, the adsorption amount of CIP also decreased significantly with the reduction in CIP^+. In particular, when the pH > 8.89, competition from –OH groups plays a major role (Hu and Wang, 2016), and the electrostatic repulsion between the CIP^- and functional groups (–CO–, –COO–, N–O– and –CN–) of UTC dominates. In general, CIP adsorption by UTC mainly involves π–π interactions, hydrogen bonding and electrostatic attraction.

3. Conclusions

With the increase in the pyrolysis temperature for the UTC preparation, the CIP adsorption ability increased initially and then decreased. UTC pyrolyzed at 450°C had excellent CIP absorption ability at 40°C and pH 6. The maximum monolayer adsorption capacity was 238.10 mg/g based on the Langmuir model. The pseudo-second-order kinetic equation agreed well with the CIP adsorption process, which was controlled by external boundary layer diffusion and intra-particle diffusion. FTIR and XPS analyses showed that –OH groups, C═C bonds of the aromatic rings, C–H groups in the aromatic rings and phenolic C–O bonds participated in the CIP adsorption process, and the N–C, N–O, O–C═O and C–OH groups of UTC were consumed in large quantities. The adsorption mechanism mainly involved π–π interactions, hydrogen bonding and electrostatic attraction. UTC pyrolyzed from UTL is a potential adsorbent material for the removal of high concentrations of CIP from aqueous solutions, and it provides a feasible approach for the utilization of UTL with high added value.

Acknowledgments

The authors acknowledge the financial support of the Industry Leading Key Projects of Fujian Province (No. 2015H0044), the Key Project of Young Talent of Institute of Urban Environment, Chinese Academy of Sciences (No. IUEZD201402), the China-Japanese Research Cooperative Program (No. 2016YFE0118000), and the Scientific and Technological Major Special Project of Tianjin City (No. 16YFXTSF00420).

REFERENCES

Alahabadi, A., Moussavi, G., 2017. Preparation, characterization and atrazine adsorption potential of mesoporous carbonate-induced activated biochar (CAB) from Calligonum Comosum biomass: parametric experiments and kinetics, equilibrium and thermodynamic modeling. J. Mol. Liq. 242, 40–52.

Alahabadi, A., Hosseini-Bandegharaei, A., Moussavi, G., Amin, B., Rastegar, A., Karimi-Sani, H., et al., 2007. Comparing adsorption properties of NH_4Cl-modified activated carbon towards chlortetracycline antibiotic with those of commercial activated carbon. J. Mol. Liq. 232, 367–381.

Angin, D., 2013. Effect of pyrolysis temperature and heating rate on biochar obtained from pyrolysis of safflower seed press cake. Bioresour. Technol. 128, 593–597.

Bartolozzi, I., Rizzi, F., Frey, M., 2017. Are district heating systems and renewable energy sources always an environmental win-win solution? A life cycle assessment case study in Tuscany, Italy. Renew. Sust. Energ. Rev. 80, 408–420.

Chang, K.L., Chen, C.C., Lin, J.H., Hsien, J.F., Wang, Y., Zhao, F., et al., 2014. Rice straw-derived activated carbons for the removal of carbofuran from an aqueous solution. New Carbon Mater. 29, 47–54.

Cheung, W.H., Szeto, Y.S., McKay, G., 2007. Intraparticle diffusion processes during acid dye adsorption onto chitosan. Bioresour. Technol. 98, 2897–2904.

Dementjev, A.P., de Graaf, A., van de Sanden, M.C.M., Maslakov, K.I., Naumkin, A.V., Serov, A.A., 2000. X-ray photoelectron spectroscopy reference data for identification of the C_3N_4 phase in carbon–nitrogen films. Diam. Relat. Mater. 9, 1904–1907.

Diao, Z.H., Xu, X.R., Jiang, D., Liu, J.J., Kong, L.J., Li, G., et al., 2017. Simultaneous photocatalytic Cr (VI) reduction and ciprofloxacin oxidation over TiO_2/FeO composite under aerobic conditions: performance, durability, pathway and mechanism. Chem. Eng. J. 315, 167–176.

El-Shafey, E.S.I., Al-Lawati, H., Al-Sumri, A.S., 2012. Ciprofloxacin adsorption from aqueous solution onto chemically prepared carbon from date palm leaflets. J. Environ. Sci. 24, 1579–1586.

Eroglu, H., Yapici, S., Nuhoglu, C., Varoglu, E., 2009. An environmentally friendly process; adsorption of radionuclide Tl-201 on fibrous waste tea. J. Hazard. Mater. 163, 607–617.

Espinosa, K., Park, J.A., Gerrity, J.J., Buono, S., Shearer, A., Dick, C., et al., 2015. Fluoroquinolone resistance in Neisseria gonorrhoeae after cessation of ciprofloxacin usage in San Francisco: using molecular typing to investigate strain turnover. Sex. Transm. Dis. 42, 57–63.

Fan, S.S., Tang, J., Wang, Y., Li, H., Zhang, H., Tang, J., et al., 2016. Biochar prepared from co-pyrolysis of municipal sewage sludge and tea waste for the adsorption of methylene blue

from aqueous solutions: kinetics, isotherm, thermodynamic and mechanism. J. Mol. Liq. 220, 432–441.
Fernandez, M.E., Ledesma, B., Roman, S., Bonelli, P.R., Cukierman, A.L., 2015. Development and characterization of activated hydrochars from orange peels as potential adsorbents for emerging organic contaminants. Bioresour. Technol. 183, 221–228.
Ghasemi, J., Asadpour, S., 2007. Thermodynamics' study of the adsorption process of methylene blue on activated carbon at different ionic strengths. J. Chem. Thermodyn. 39, 967–971.
Gupta, V.K., Gupta, B., Rastogi, A., Agarwal, S., Nayak, A., 2011. A comparative investigation on adsorption performances of mesoporous activated carbon prepared from waste rubber tire and activated carbon for a hazardous azo dye—Acid Blue 113. J. Hazard. Mater. 186, 891–901.
Han, L., Ro, K.S., Sun, K., Sun, H., Wang, Z., Libra, J.A., et al., 2016. New evidence for high sorption capacity of hydrochar for hydrophobic organic pollutants. Environ. Sci. Technol. 50, 13274–13282.
He, H.J., Xiang, Z.H., Chen, X.J., Chen, H., Huang, H., Wen, M., et al., 2017. Biosorption of Cd(II) from synthetic wastewater using dry biofilms from biotrickling filters. Int. J. Environ. Sci. Technol. https://doi.org/10.1007/s13762-017-1507-8.
Hu, D., Wang, L., 2016. Adsorption of ciprofloxacin from aqueous solutions onto cationic and anionic flax noil cellulose. Desalin. Water Treat. 57, 28436–28449.
Huang, Y., Ma, E., Zhao, G., 2015. Thermal and structure analysis on reaction mechanisms during the preparation of activated carbon fibers by KOH activation from liquefied wood-based fibers. Ind. Crop. Prod. 69, 447–455.
Jiang, J., Zhang, L., Wang, X., Holm, N., Rajagopalan, K., Chen, F., et al., 2013. Highly ordered macroporous woody biochar with ultra-high carbon content as supercapacitor electrodes. Electrochim. Acta 113, 481–489.
Keiluweit, M., Kleber, M., 2009. Molecular-level interactions in soils and sediments: the role of aromatic π-systems. Environ. Sci. Technol. 43, 3421–3429.
Kicinski, W., Norek, M., Jankiewicz, B.J., 2014. Heterogeneous carbon gels: N-doped carbon xerogels from resorcinol and N-containing heterocyclic aldehydes. Langmuir 30, 14276–14285.
Li, M., Wei, D., Du, Y., 2014. Acute toxicity evaluation for quinolone antibiotics and their chlorination disinfection processes. J. Environ. Sci. 26, 1837–1842.
Li, X.N., Chen, S., Fan, X.F., Quan, X., Tan, F., Zhang, Y.B., et al., 2015a. Adsorption of ciprofloxacin, bisphenol and 2-chlorophenol on electrospun carbon nanofibers: in comparison with powder activated carbon. J. Colloid Interface Sci. 447, 120–127.
Li, X., Li, F., Jin, Y., Jiang, C., 2015b. The uptake of uranium by tea wastes investigated by batch, spectroscopic and modeling techniques. J. Mol. Liq. 209, 413–418.
Liao, X., Li, B., Zou, R., Dai, Y., Xie, S., Yuan, B., 2016. Biodegradation of antibiotic ciprofloxacin: pathways, influential factors, and bacterial community structure. Environ. Sci. Pollut. Res. Int. 23, 7911–7918.
Malkoc, E., Nuhoglu, Y., 2006. Removal of Ni(II) ions from aqueous solutions using waste of tea factory: adsorption on a fixed-bed column. J. Hazard. Mater. 135, 328–336.
Mao, H., Wang, S., Lin, J.Y., Wang, Z., Ren, J., 2016. Modification of a magnetic carbon composite for ciprofloxacin adsorption. J. Environ. Sci. 49, 179–188.
Moniruzzaman, M., Ono, T., 2013. Separation and characterization of cellulose fibers from cypress wood treated with ionic liquid prior to laccase treatment. Bioresour. Technol. 127, 132–137.
Nasuha, N., Hameed, B.H., Din, A.T.M., 2010. Rejected tea as a potential low-cost adsorbent for the removal of methylene blue. J. Hazard. Mater. 175, 126–132.
Pang, X., Ran, X., Kuang, F., Xie, J., Hou, B., 2010. Inhibiting effect of ciprofloxacin, norfloxacin and ofloxacin on corrosion of mild steel in hydrochloric acid. Chin. J. Chem. Eng. 18, 337–345.
Peng, C., Yan, X.b., Wang, R.T., Lang, J.W., Ou, Y.J., Xue, Q.J., 2013. Promising activated carbons derived from waste tea-leaves and their application in high performance supercapacitors electrodes. Electrochim. Acta 87, 401–408.
Peng, X.M., Hu, F.P., Lam, F.L.Y., Wang, Y.J., Liu, Z.M., Dai, H.L., 2015. Adsorption behavior and mechanisms of ciprofloxacin from aqueous solution by ordered mesoporous carbon and bamboo-based carbon. J. Colloid Interface Sci. 460, 349–360.
Peng, X.M., Hu, F.P., Huang, J.L., Wang, Y.J., Dai, H.L., Liu, Z.M., 2016. Preparation of a graphitic ordered mesoporous carbon and its application in sorption of ciprofloxacin: kinetics, isotherm, adsorption mechanisms studies. Microporous Mesoporous Mater. 228, 196–206.
Plomp, A.J., Su, D.S., Jong, K.P.d., Bitter, J.H., 2009. On the nature of oxygen-containing surface groups on carbon nanofibers and their role for platinum deposition—an XPS and titration study. J. Phys. Chem. C 113, 9865–9869.
Rajapaksha, A.U., Vithanage, M., Zhang, M., Ahmad, M., Mohan, D., Chang, S.X., et al., 2014. Pyrolysis condition affected sulfamethazine sorption by tea waste biochars. Bioresour. Technol. 166, 303–308.
Shen, B., Tian, L., Li, F., Zhang, X., Xu, H., Singh, S., 2017. Elemental mercury removal by the modified bio-char from waste tea. Fuel 187, 189–196.
Srivastava, V.C., Swamy, M.M., Mall, I.D., Prasad, B., Mishra, I.M., 2006. Adsorptive removal of phenol by bagasse fly ash and activated carbon: equilibrium, kinetics and thermodynamics. Colloids Surf. A Physicochem. Eng. Asp. 272, 89–104.
Sun, Y.Y., Li, H., Li, G.C., Gao, B.Y., Yue, Q.Y., Li, X.B., 2016. Characterization and ciprofloxacin adsorption properties of activated carbons prepared from biomass wastes by H_3PO_4 activation. Bioresour. Technol. 217, 239–244.
Trivedi, P., Vasudevan, D., 2007. Spectroscopic investigation of ciprofloxacin speciation at the goethite–water interface. Environ. Sci. Technol. 41, 3153–3158.
Tu, J., Yang, Z., Hu, C., Qu, J., 2014. Characterization and reactivity of biogenic manganese oxides for ciprofloxacin oxidation. J. Environ. Sci. 26, 1154–1161.
Uzun, B.B., Apaydin-Varol, E., Ateş, F., Özbay, N., Pütün, A.E., 2010. Synthetic fuel production from tea waste: characterisation of bio-oil and bio-char. Fuel 89, 176–184.
Vithanage, M., Mayakaduwa, S.S., Herath, I., Ok, Y.S., Mohan, D., 2016. Kinetics, thermodynamics and mechanistic studies of carbofuran removal using biochars from tea waste and rice husks. Chemosphere 150, 781–789.
Wang, F.M., Ma, X.L., Bian, W.T., Ren, L.J., Wang, Y.J., Duan, J.Y., et al., 2016. The adsorption characteristic of reservior sediment to ciprofloxacin (in Chinese). J. Soil Water Conserv. 30, 312–316.
Yang, C.P., Wang, J.Q., Lei, M., Xie, G.X., Zeng, G.M., Luo, S.L., 2010. Biosorption of zinc(II) from aqueous solution by dried activated sludge. J. Environ. Sci. 22, 675–680.
Yang, W., Lu, Y., Zheng, F., Xue, X., Li, N., Liu, D., 2012. Adsorption behavior and mechanisms of norfloxacin onto porous resins and carbon nanotube. Chem. Eng. J. 179, 112–118.
Zhang, Y.J., Xing, Z.J., Duan, Z.K., Meng, L., Wang, Y., 2014. Effects of steam activation on the pore structure and surface chemistry of activated carbon derived from bamboo waste. Appl. Surf. Sci. 315, 279–286.
Zhang, B., Han, X., Gu, P., Fang, S., Bai, J., 2017. Response surface methodology approach for optimization of ciprofloxacin adsorption using activated carbon derived from the residue of desilicated rice husk. J. Mol. Liq. 238, 316–325.
Zhu, L.G., Cheng, X.X., Zhang, W.J., Wu, Z.D., Jiang, F.Y., 2013. Research progress on the reuse of solid waste in tea industry and its application in environment improvement (in Chinese). Fujian J. Agric. Sci. 28, 1310–1315.